Mineral Mapping at Cuprite, Nevada with a 63-Channel Imaging Spectrometer

F. A. Kruse, K. S. Kierein-Young, and J. W. Boardman
Center for the Study of Earth from Space (CSES), Cooperative Institute for Research in Environmental Sciences (CIRES),
University of Colorado, Boulder, CO 80309-0449

ABSTRACT: Geophysical and Environmental Research Imaging Spectrometer (GERIS) 63-channel scanner data covering the spectral region 0.4 to 2.5 μm were analyzed for the Cuprite mining district, Esmeralda and Nye Counties, Nevada. The data were calibrated to reflectance using field spectral measurements. Individual and spatially averaged spectra extracted from the GERIS data were used to identify the minerals alunite, kaolinite, buddingtonite, and hematite by their spectral characterisitcs. An area with reflectance properties similar to zeolite-group minerals was also identified. The images were classified in the spectral domain to produce color-coded image maps of mineral distribution that clearly show the zoned nature of the hydrothermal system. Comparison of the thematic mineral maps with existing geologic and alteration maps demonstrates the utility of imaging spectrometers for producing detailed maps for mineral exploration. Identification of individual minerals and spatial display of the dominant mineralogy using the imaging spectrometer data adds information that can be used in determining the morphology and genetic origin of the district.

INTRODUCTION

THE OBJECTIVE OF THIS RESEARCH was both to evaluate the GERIS and to use the data to develop a better understanding of the hydrothermal system at Cuprite, Nevada. Detailed maps of the distribution of materials at the surface are essential to understanding the Earth as dynamic system. High spectral resolution remote sensing (imaging spectrometry) is a new tool that can be used to quickly produce detailed maps for previously unmapped areas, and to supplement existing geologic mapping. Imaging spectrometry is "the simultaneous acquisition of images in many narrow, contiguous spectral bands" (Goetz et al., 1985). Analysis of imaging spectrometer data allows extraction of a detailed spectrum for each picture element (pixel) of the image. Broad-band remote sensing systems, such as the Landsat Multispectral Scanner (MSS) and Landsat Thematic Mapper (TM), drastically under sample the information content available from a reflectance spectrum. An imaging spectrometer, on the other hand, samples at close intervals and allows construction of spectra that closely resemble those measured on laboratory instruments (Figure 1). The high spatial and spectral resolution imaging spectrometer systems make identification of individual minerals (alunite, calcite, dolomite, kaolinite, muscovite, etc.) and mineral assemblages possible (Marsh and McKeon, 1983; Goetz et al., 1985; Lang et al., 1987; Kruse, 1988; Pieters and Mustard, 1988).

The first imaging spectrometer, the Airborne Imaging Spectrometer (AIS), was designed at the Jet Propulsion Laboratory and flown during the 1984 through 1986 flight seasons on NASA's C-130 aircraft. The AIS was an experimental instrument designed to test two-dimensional, near-infrared area array detectors, imaging 128 bands from 1.2 to 2.4 μm (Vane et al., 1983). Several investigators have reported on the varied geologic applications of the AIS data (Vane and Goetz, 1985, 1986; Vane, 1987a). Goetz et al. (1985) and Goetz and Srivastava (1985) used the AIS data to identify the minerals kaolinite and alunite at Cuprite, Nevada, and to produce narrow strip maps showing their distribution for a portion of the mining district.

The Airborne Visible/Infrared Imaging Spectrometer (AVIRIS) represents the second generation of NASA imaging spectrometers. It is a 224-channel instrument utilizing the spectral range 0.41 to 2.45 μm in approximately 10-nm-wide bands (Porter and Enmark, 1987). Preliminary geologic results have been reported by Vane (1987b) for images of Cuprite. Individual spectra of the minerals kaolinite, alunite, and buddingtonite were successfully
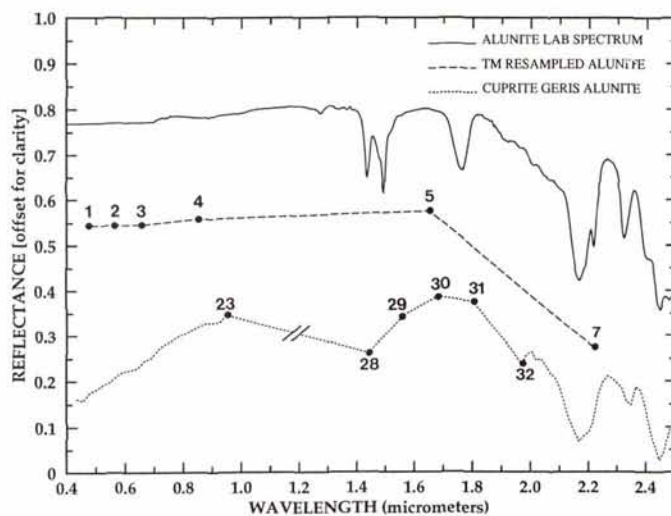

FIG. 1. Comparison of a laboratory spectrum of alunite (Sulfur, California), a simulated Thematic Mapper (TM) spectrum (resampled from the lab spectrum), and a GERIS spectrum from Cuprite, Nevada. Symbols and channel numbers on both the TM and GERIS spectra indicate band centers of widely spaced, broad scanner channels (note that channels 24 to 27 (0.971 to 1.32 μm) have been deleted in the GERIS data because of poor scanner performance characteristics). Other data points on the GERIS spectrum are too close together to mark. Note that all characteristic absorption band information is lost with the TM spectrum (with the exception of low reflectance in TM band 7 at 2.2 μm), while much of the spectral information is preserved in the GERIS spectrum. The spectra are offset vertically for clarity and the absolute values of the reflectance axis do not show true brightness.

extracted from the AVIRIS data, but no map showing the mineral distributions was produced for the district.

Based in part on the success of the NASA instruments and on demand from the mining and petroleum industries, Geophysical and Environmental Research Corporation (GER) developed a 63-channel high spectral resolution scanner for commercial use (a 64th channel is used to store aircraft gyroscopic information). The system consists of three grating spectrometers with three individual linear detector arrays (Figure 2.) The GER imaging spectrometer (GERIS) qualifies as an imaging spectrometer
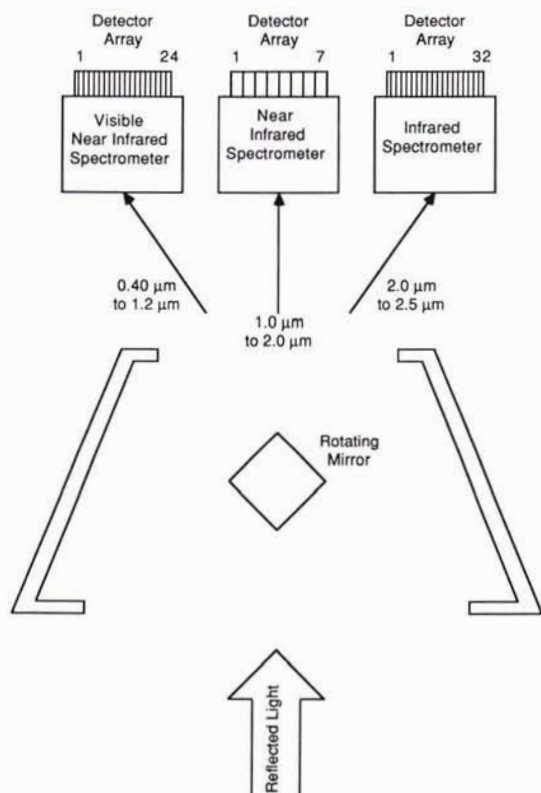
FIG. 2. Block diagram of GERIS optics (modified from William Collins, written communication, 1989).

FIG. 3. Generalized geologic map for the Cuprite mining district. Modified from Kahle and Goetz (1985) and Abrams et al. (1977).

TABLE 1.   GERIS BAND SPECIFICATIONS

Wavelength range	Number of channels	Sampling Interval
0.4 - 1.0 μm	24	23 nm
1.0 - 2.0 μm	7	120 nm
2.0 - 2.5 μm	32	17 nm

in the true sense of the definition as it acquires 63 inherently co-registered data channels simultaneously, produces continuous spectra, and retains the image format. It differs from other imaging spectrometers, however, in that the spectral bands vary in width across the spectrum (Table 1). These bands were selected to provide maximum signal-to-noise while retaining sufficient spectral resolution to identify key minerals (William Collins, written communication, 1987).

The GERIS is flown on a Piper Aztec twin engine aircraft at an altitude of about 20,000 ft. A 90 degree scan using a rotating mirror provides a selectable swath width of 512 or 1024 pixels and the along-flightline dimension is provided by the aircraft's forward motion. Data are recorded directly on 6250 BPI computer compatible tapes as 16-bit integers and, after calibration to radiance, are typically provided by GER as 63 single-band, band sequential (BSQ) images. GER claims radiometric calibration repeatability to within 1 percent from flight to flight (William Collins, written communication, 1989).

GEOLOGY AND ALTERATION

The Cuprite mining district is located about 15 km south of Goldfield on U.S. Highway 95 in southwest Nevada (Figure 3). The geology of the district is relatively well known and has been described in detail by Abrams *et al.* (1977), Ashley and Abrams
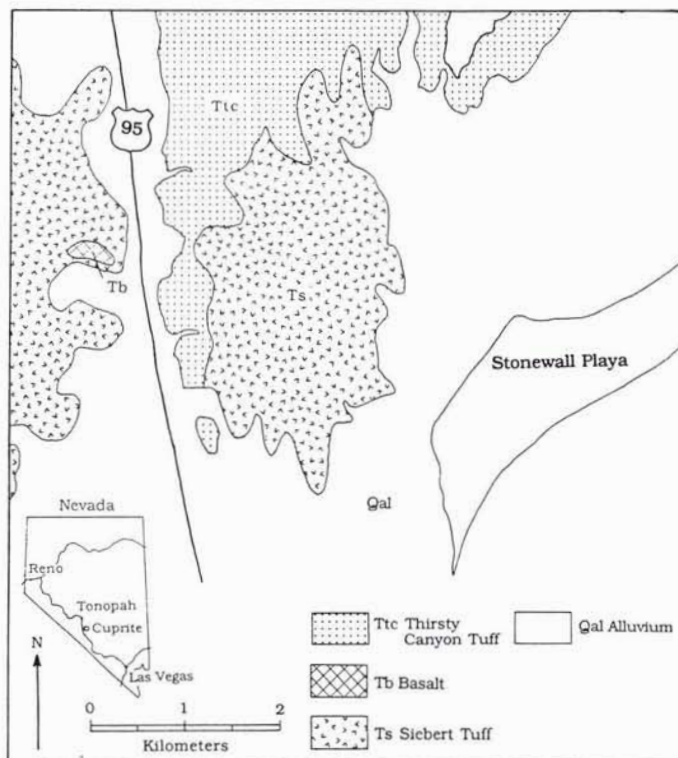
(1980), and Shipman and Adams (1987). Bedrock in the area consists of Tertiary volcanic and volcaniclastic rocks, principally rhyolitic ash-flow tuffs with some air-fall tuff (Abrams et al., 1977). Cambrian clastic and carbonate sedimentary rocks are exposed east of Highway 95 just outside the study area. The volcanic rocks have been extensively modified in the Cuprite district by hydrothermal alteration. Ashley and Abrams (1980) identified three mappable zones of alteration consisting of an intensely altered central silica cap surrounded by subsequently less altered zones of opalized and argillized rock (Figure 4). The mineralogy in the silicified zone was observed to the primarily quartz with minor calcite, alunite, and kaolinite. The opalized rocks contain the alteration minerals opal, alunite, and kaolinite. The argillized zone mineralogy consists of kaolinite derived from plagioclase, and montmorillonite and opal derived from volcanic glass.

SPECTRAL MAPPING

GENERAL

Cuprite has been used for many remote sensing studies over the years. An extensive image database and a collection of field and laboratory spectra exist for the district (Rowan *et al.*, 1974; Abrams *et al.*, 1977; Ashley and Abrams, 1980; Kahle and Goetz, 1983; Goetz *et al.*, 1985; Curtiss *et al.*, 1985, Shipman and Adams, 1987). The Cuprite site, although not known to be economically mineralized, is an excellent area to test remote sensing technology because of the good rock exposures and the presence of several distinct mineral assemblages.

The Geophysical and Environmental Research 63-channel imaging spectrometer (GERIS) was flown over Cuprite during August 1987. Plate 1 is a "true" color composite image of GERIS bands 11, 6, and 4 (0.67 μm, 0.55 μm, and 0.50 μm) (RGB) showing the area covered by the flight. Note that this image

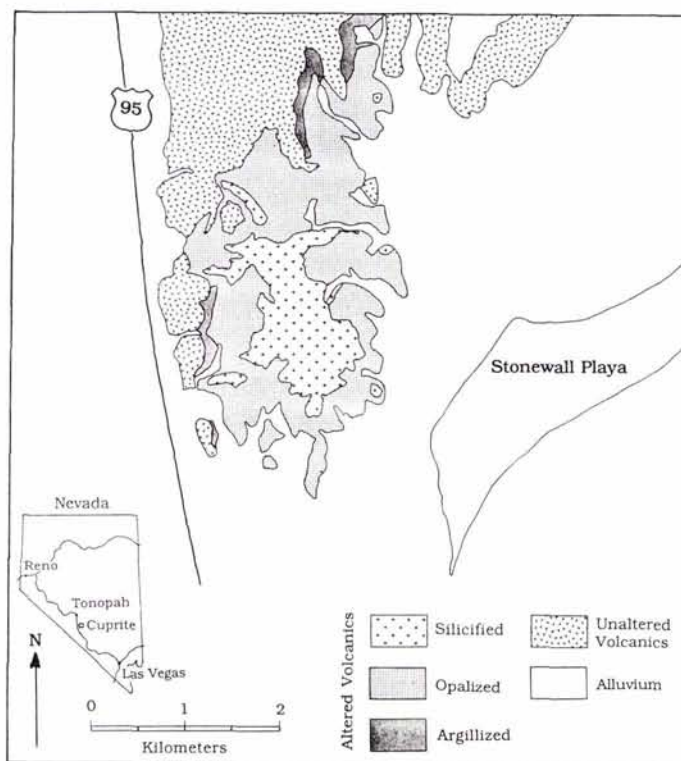FIG. 4. Alteration map for the Cuprite mining district. Redrawn from Shipman and Adams (1987) after Abrams *et al.* (1977).

by International Imaging Systems). This combination allows simultaneous display of three spatial image planes as a color composite image on the IVAS display with a side slice showing the spectral dimension, and real-time display of spectra on the GPX graphics screen. A vertical line-cursor on the IVAS display shows the location of the spectral slice, while a standard crosshair-cursor shows the location of the current spectrum. Concurrent application processes allow selection of ground targets for calibration, extraction of average spectra, and spectral classification. We are developing concurrent ISIS analysis programs that utilize expert system capabilities (Kruse *et al.*, 1988) and allow spectral unmixing to be used in the image classification (Boardman, 1989).

Several investigators are developing alternate techniques for extraction of spectral information from imaging spectrometer data. One common approach relies on removal of a continuum from the data and automated extraction of spectral information (Green and Craig, 1985; Kruse *et al.*, 1985, 1986; Kruse, 1987, 1988; Yamaguchi and Lyon, 1986; and Clark *et al.*, 1987). Automatic absorption feature extraction algorithms allow objective characterization of absorption bands in terms of quantities such as band position, depth, full width at half the maximum depth (FWHM), and asymmetry. Absorption features have been successfully extracted and characterized for both laboratory and aircraft spectra (Clark *et al.*, 1987; Kruse *et al.*, 1988); however, these techniques have met with limited success for image classification thus far, primarily because they are sensitive to signal-to-noise ratios of the data. Other algorithms for identification of spectral mixtures and deconvolution of mixed spectra are being developed by Mustard and Pieters (1986, 1987) and Smith and Adams (1985).

CALIBRATION

Analysis of imaging spectrometer data requires that both wavelength and radiometric calibration be performed. These steps were accomplished as preprocessing operations prior to analysis using the ISIS software. Laboratory measurements by GER provided the initial wavelength calibration for the Cuprite GERIS data. An additional check on the wavelength calibration was made by comparing the positions of known atmospheric absorption features to their locations in the imaging spectrometer data. Atmospheric carbon dioxide (CO_2) absorption bands located at 2.005 and 2.055 µm were useful for wavelength-calibration of the data in the infrared (Kneisyz *et al.*, 1980; Vane, 1987b). The corresponding CO_2 absorption bands were observed in the GERIS radiance data at 2.0189 and 2.0682 µm, respectively, offset $+0.0139$ and $+0.0132$ µm or approximately 1 channel from where they should be located. Accordingly, the wavelength positions were adjusted 1 channel in the last spectrometer to shift the CO_2 bands to their proper spectral positions. Atmospheric H_2O absorption bands in the visible portion of the spectrum were also examined to determine if they were properly located in the GERIS data. Unfortunately, these features are not as sharp as those in the infrared, and the GERIS channels are more broadly spaced in this region. The observed positions of the 0.66, 0.76, and 0.94 µm atmospheric absorption features in the GERIS data were within 1 or 2 channels of their correct positions; however, their exact location oscillated, and offset directions were inconsistent. Therefore, the visible wavelengths provided by GER were used as the correct channel wavelengths.

The next and most critical step in the data reduction is to convert the data to reflectance so that individual spectra can be compared directly with laboratory data for mineral identification. Ideally, the aircraft data should be calibrated to absolute reflectance; however, this requires onboard calibration to reflectance for each flight, which is not available for the GERIS data. In the absence of onboard calibration, two standard areas on the ground were used to calibrate the data (Roberts *et al.*,
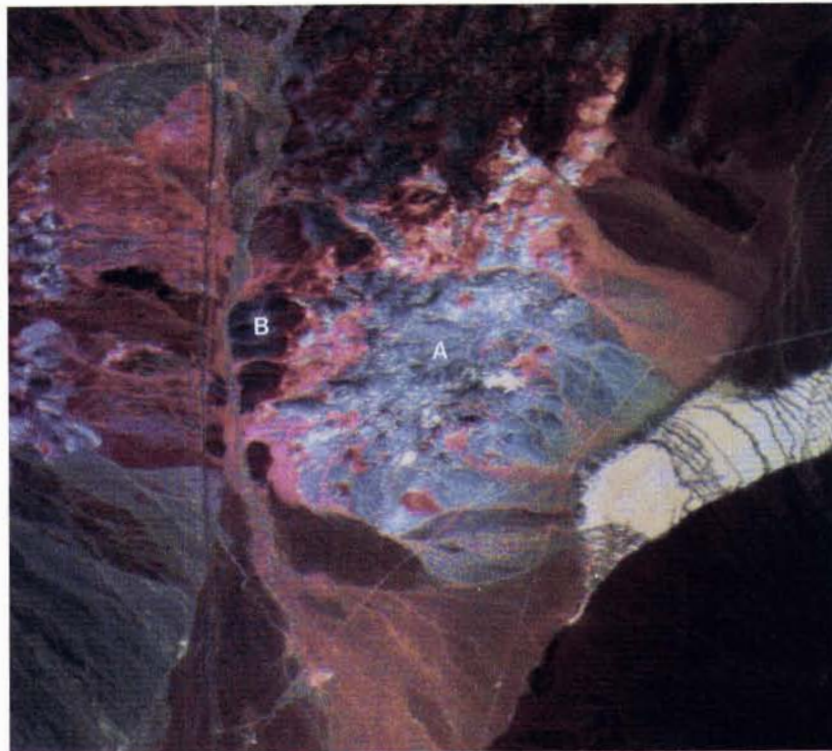
has not been geometrically corrected and thus the orientation and geometry of the image does not exactly match that of the geologic and alteration maps shown in Figures 3 and 4. Spatial resolution of each pixel is about 12 metres cross track and about 22 metres down track. Comparison of the image with the maps is facilitated by noting the locations and geometry of U.S. Highway 95 near the left edge of the image and the bright Stonewall Playa near the center of the right edge. The color contrast of this image has been enhanced through the use of "saturation enhancement" to improve the color saturation or purity (Kruse and Raines, 1984; Gillespie *et al.*, 1986). The altered rocks (A) are easily distinguished from the unaltered rocks (B), primarily because of the apparent bleaching of the altered rocks. Note, however, that even on an enhanced color composite little detail is available for discriminating alteration mineralogy. The three alteration zones mapped by Ashley and Abrams (1980) are not readily apparent. Commonly used techniques such as principal components or band ratioing would serve to enhance the spectral differences; however, they do not take full advantage of the spectral information available nor of the determinative nature of imaging spectrometer data.

ANALYSIS SOFTWARE

Complete analysis of imaging spectrometer data requires sophisticated image processing techniques that combine simultaneous extraction and display of both spectral and spatial information. Analysis software is under development at several research facilities that takes advantage of the combined high resolution graphics and imaging capabilities of modern image processing workstations (Mazer *et al.*, 1987, 1988; Torson, 1989). An analysis package called "Integrated Software for Imaging Spectrometers" (ISIS) (Torson, 1989) was used for the analysis of the Cuprite GERIS data. ISIS runs on a Digital Equipment Corporation (DEC) VAXstation with GPX color graphics display configured with an additional 1024 by 1024 image display (IVAS,

PLATE. 1. Saturation enhanced color composite image of GERIS bands 11, 6, and 4 (0.67 μm, 0.55 μm, and 0.50 μm) (RGB) showing the area covered by the flight. Altered volcanic rocks (A) are distinguishable from unaltered volcanic rocks (B) primarily because of bleaching.

1985; Elvidge 1988). This approach requires *a priori* knowledge of each site. This empirical correction uses a constant gain and offset for each band to force a best fit, in the least-squares sense, between sets of field spectra and image spectra characterizing the same ground areas. The result of this calibration is the removal of atmospheric effects (both attenuation and scattering), viewing geometry effects, and any residual instrument artifacts. While no such correction can be perfect, it does allow conversion of the remotely sensed spectra into a form that can be readily compared with laboratory or field acquired spectra.

The calibration to reflectance, as we have implemented it, is a three-step process. The first involves choosing two ground target regions and acquiring field spectra to characterize them. These regions should span a wide albedo range. Field spectra were measured and samples were collected for several areas at the Cuprite site during 1988. For this study, the two calibration targets used were Stonewall playa (bright target) and a varnished tuff (dark target). The second step in the process involves picking the multiple pixels in the airborne data set that are associated with each ground target. This is done interactively, and individual pixels are selected until the regions are fully covered. Then, an over determined system of linear equations may be constructed for each band in which the number of unknowns is two, the gain and offset values, and the number of knowns is equal to the total number of image pixels chosen. Solving these systems of equations provides gain and offset spectra for use in the calibration, as well as estimations of the standard error for each parameter at each wavelength (Figures 5 and 6). Large total errors in the estimates produced during the calibration process may indicate excessive spatial variability or potentially, instrument instability. For the Cuprite data, channels 24 through 27 (0.971 to 1.32 μm) had excessively high total errors and were deleted
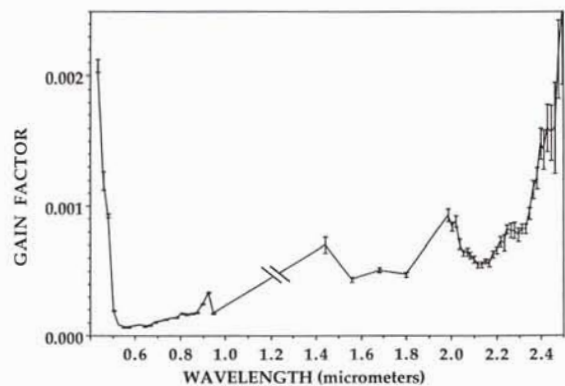

FIG. 5. Gain factor spectrum of Cuprite GERIS data with standard errors superimposed. Bands 24 through 27 (0.971 to 1.32 μm) have been deleted due to high error.

from further analysis. The gain spectrum of the remaining bands is essentially an inverse solar irradiance curve. The gains are highest in the extreme wavelengths and in the regions of water absorption. The standard errors of the gain factors are also highest in these regions. The offset value spectrum is a negative correction that increases in magnitude with wavelength. This is most likely a correction for some residual dark current in the instrument. The correction implies that a zero reflectance target would have a positive DN value in the uncorrected data that would increase with wavelength.

The final step in the calibration involves the actual correction of the data. The instrument DN values are multiplied by the
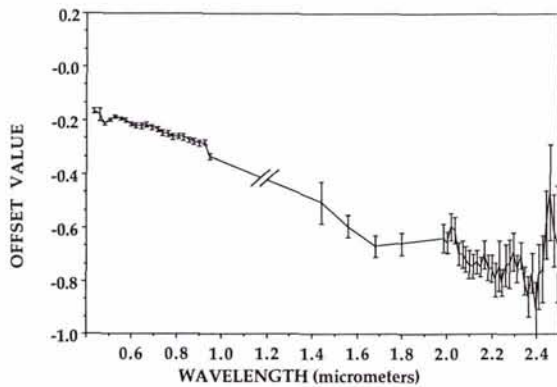
FIG. 6. Offset value spectrum for Cuprite GERIS data with standard errors superimposed. Bands 24 through 27 (0.971 to 1.32 μm) have been deleted due to high error.

proper gain factor, and the corresponding offset value is added. These gain and offset corrections may be applied to any or all of the total imaging spectrometer data set. The outputs from this process are the original DN spectra empirically corrected to reflectance spectra. In this corrected form direct comparison to laboratory and field reflectance spectra can be made. The empirical method used here for correction to reflectance is a rapid and easily implemented technique. It corrects for atmospheric, instrument, and viewing geometry effects. It also provides error estimates for each band on the accuracy of the calibration, which can be used in all subsequent processing. The technique does require field or laboratory spectra of at least two regions in the area of interest. It also makes the assumption that all of the image pixels chosen to characterize each ground spectrum represent identical composition and reflectance response. Currently we are investigating the effect of including more than two ground targets, in an attempt to remove any residual instrument calibration errors. This will require a fitting of a nonlinear response for each band.

SPECTRAL CLASSIFICATION

Once reflectance spectra have been obtained, the sheer volume of the data requires that efficient algorithms for mineral identification be utilized to analyze the data. One approach involves binary encoding and spectral matching using a reference library (Mazer et al., 1987, 1988). Each reference spectrum is encoded by finding its mean and determining whether each point in the spectrum is above or below the mean. The spectrum is stored as an integer value with each bit representing a point in the spectrum. If a point is above or equal to the mean it is set to 1 and if a point is below the mean it is set to 0. The spectrum for each pixel in the image is encoded in the same manner and compared to the reference spectrum using a bitwise exclusive OR. The exclusive OR determines points where the encoded spectra do not match. A tolerance is used to determine how many points in the spectra must match in order to classify that pixel as being a match to the reference. Binary encoding is a fast and accurate technique for identifying minerals with distinct absorption bands because it is sensitive to band positions and insensitive to albedo (brightness) variation.

For the Cuprite GERIS data, the binary encoding technique was used to find the distribution of three minerals in the Cuprite image. Spectra (averages of 3 by 3 boxes) from known locations of alunite, buddingtonite (an ammonium feldspar (Krohn and Altaner, 1987)), and kaolinite were extracted from the Cuprite data using the ISIS software and used as references for the classification. Only the 32 bands in the infrared region between 1.9 and 2.5 μm were used in the binary encoding because they

contain the most information for these minerals. Figures 7, 8, and 9 show the spectra extracted from the GERIS data compared to laboratory standards and to laboratory spectral measurements of samples collected at Cuprite. The spectra extracted from the GERIS images provided the ability to identify individual minerals by their spectral characteristics. Alunite was identified by the presence of a broad 2.16 μm absorption band and weaker bands near 2.32 and 2.42 μm (Figures 7 and 10). Kaolinite was identified by the presence of an asymmetrical band at 2.20 μm. Figures 8 and 10 show how the GERIS spectral resolution of 17 nm in the 2.0- to 2.5-μm spectral region results in an asymmetrical single band at 2.20 μm rather than the characteristic 2.16-μm and 2.20-
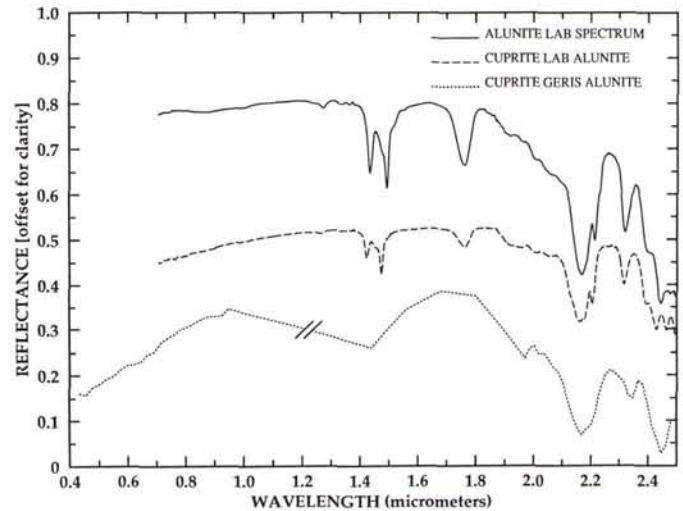

FIG. 7. Comparison of a laboratory spectrum of alunite (Sulfur, California), a laboratory spectrum from Cuprite, and a Cuprite GERIS spectrum identified as alunite. The spectra are offset vertically for clarity and the absolute values of the reflectance axis do not show true brightness. X-Ray diffraction verifies the aircraft identification (Kruse, unpublished data, 1989).
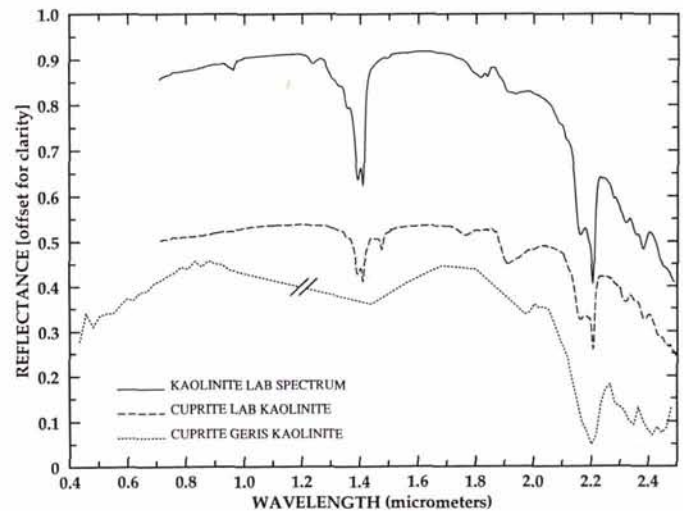

FIG. 8. Comparison of a laboratory spectrum of kaolinite (Washington County, Georgia), a laboratory spectrum from Cuprite, and a Cuprite GERIS spectrum identified as kaolinite. The spectra are offset vertically for clarity and the absolute values of the reflectance axis do not show true brightness. A small absorption band near 1.75 μm in the laboratory spectra indicates the presence of intermixed alunite. X-Ray diffraction verifies the aircraft identification (Kruse, unpublished data, 1989).
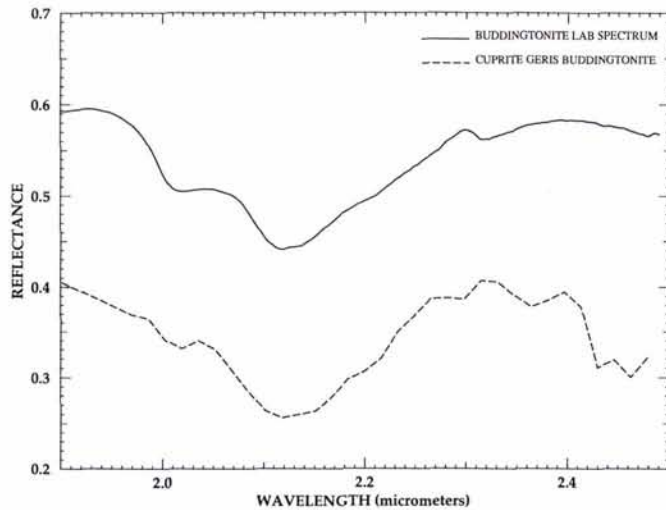
FIG. 9. Comparison of a laboratory spectrum of buddingtonite (Menlo Park, California, sample provided by R. C. Erd) and a Cuprite GERIS spectrum identified as buddingtonite. The spectra are offset vertically for clarity and the absolute values of the reflectance axis do not show true brightness. Field spectroscopy and X-Ray diffraction verify the aircraft identification (Kruse, unpublished data, 1989).
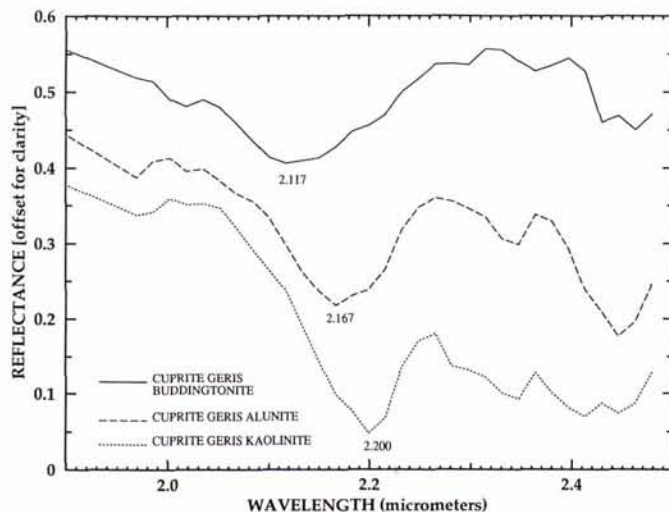

FIG. 10. Comparison of GERIS buddingtonite, alunite, and kaolinite spectra showing the locations of the strongest absorption bands. The spectra are offset vertically for clarity and the absolute values of the reflectance axis do not show true brightness.

μm kaolinite doublet seen in both of the laboratory spectra. The doublet was observed, however, in a few individual spectra. Figure 9 compares a laboratory standard for buddingtonite and a GERIS buddingtonite spectrum. The broad absorption feature at 2.117 seen in both Figures 9 and 10 is characteristic of this mineral. The distribution of these three minerals in the image is shown in Plate 2. It should be noted that this is a map of the predominant mineral (spectrally) in each pixel. Mineral mixing was not considered, although field and laboratory spectral measurements indicate that there is significant mineral mixing taking place at the surface. Mineral mixing at Cuprite, Nevada, is being studied by Boardman (1989).

Several other areas with identifiable spectral characteristics were located during the interactive analysis stage with the ISIS software. One previously unreported area with spectral

characteristics similar to zeolite-group minerals was discovered north of the main altered area in the unaltered volcanic rocks. Figure 11 compares the extracted spectrum with a laboratory spectrum for a volcanic tuff containing several zeolite minerals. The strong absorption bands at 1.4, 1.9, and near 2.45 μm are characteristic of zeolite-group minerals (Ehmann and Vergo, 1986). The apparent position of the absorption feature near 2.45 μm indicates that the predominant zeolite mineral may be natrolite (Ehmann and Vergo, 1986). This observation has not yet been field checked or confirmed by laboratory analysis.

The abundance of red areas on the color composite image (Plate 1) indicates the probable presence of iron oxide minerals at the surface. Accordingly, an average spectrum was extracted from the Cuprite data, compared to lab spectra of hematite and goethite (Figure 12), and used to classify the GERIS image. Hematite was identified by the presence of a broad absorption band near 0.85 μm in the average spectrum. Only the first 24 GERIS channels were used for classification because hematite does not have spectral features in the near-infrared. A "spectrum ratioing" technique was used to find the distribution of hematite in the Cuprite image (Plate 3). This technique classifies an image by dividing the reference spectrum by the spectrum for each pixel in the image. The resulting average deviation from 100 percent is compared to a tolerance to determine if the image spectrum matches the reference spectrum. The ratio technique was selected for classification of the hematite because the binary encoding does not work well for minerals without sharp absorption features. Unlike the binary encoding, the spectrum ratioing technique is sensitive to albedo and topographic slope as well as absorption band positions and depths.

RESULTS

Analysis of the GERIS data in the spectral domain results in extraction of absorption band information that allows definition of the surface mineralogy at Cuprite. Because complete spectra can be extracted from the imaging spectrometer data, it was possible to identify and map the individual minerals. The GERIS data show a roughly concentrically zoned hydrothermal system. The mapped mineral zones do not correspond one-for-one to Abrams' alteration zones; however, a general match is ob-
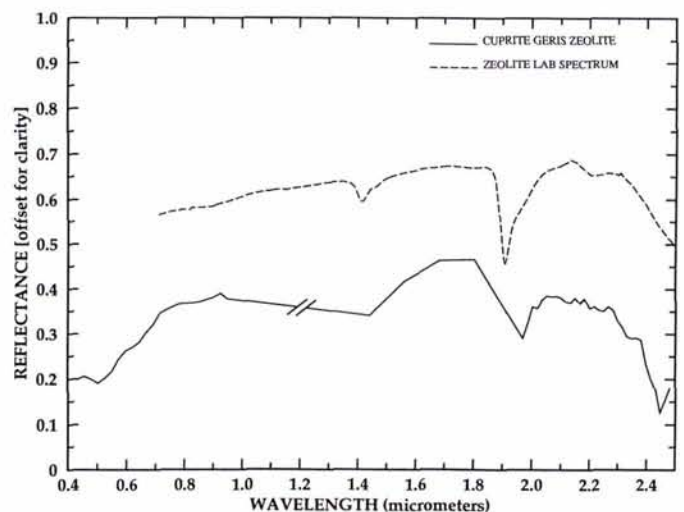

FIG. 11. Comparison of a laboratory spectrum of a mixture of several zeolite minerals from the northern Grapevine Mountains, Nevada (Kruse, 1988) and a GERIS spectrum speculated to contain zeolites. This result has not yet been verified by collection of field samples. The spectra are offset vertically for clarity and the absolute values of the reflectance axis do not show true brightness.
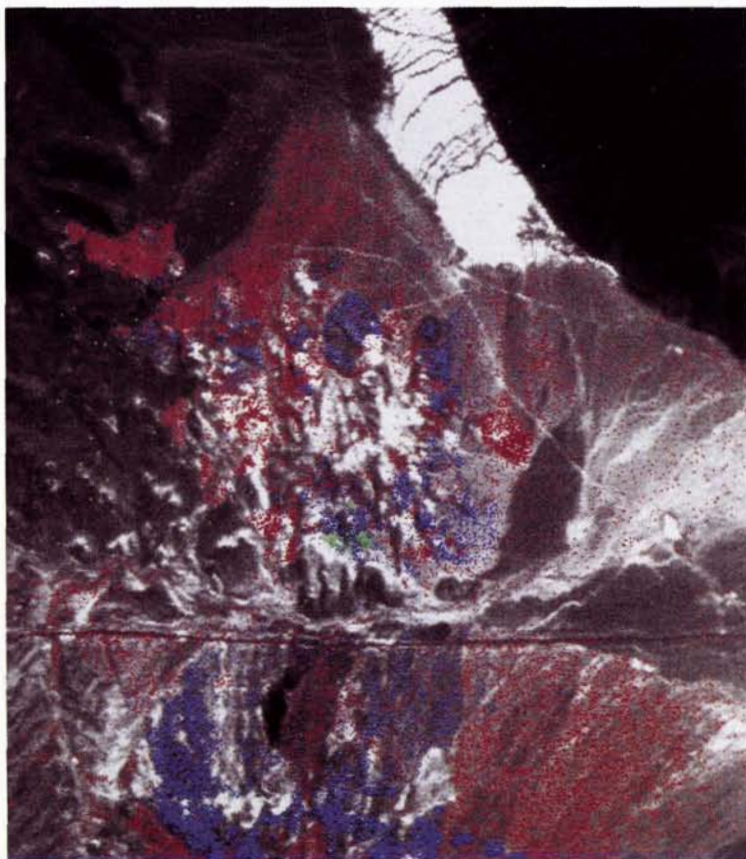
PLATE. 2. Color-coded image map of the Cuprite Mining District produced by binary encoding of and spectral matching to the GERIS spectra shown in Figures 7, 8, 9, and 10. The color codes indicate the predominant mineral in each pixel of the image; Blue pixels = alunite, Red pixels = kaolinite, Green pixels = buddingtonite. Unclassified areas are shown as the original gray scale image.
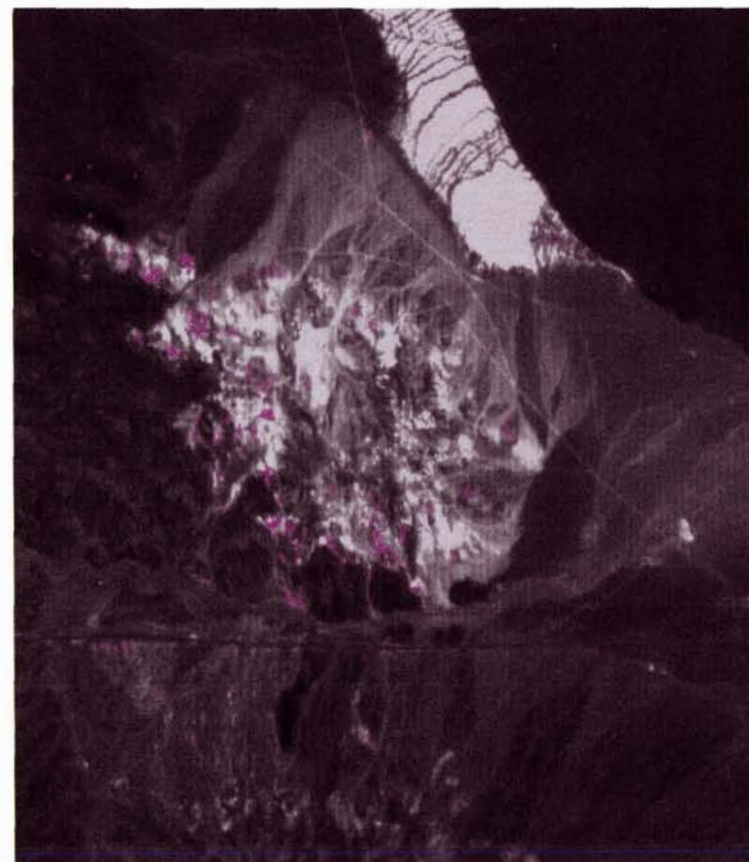

PLATE 3. Color-coded image map of the Cuprite Mining District produced by spectrum ratioing and spectral matching to the GERIS spectrum shown in Figure 12. The color code (purple) indicates the distribution of areas where hematite is spectrally dominant (in the visible portion of the spectrum) for the district. Unclassified areas are shown as the original gray scale image.
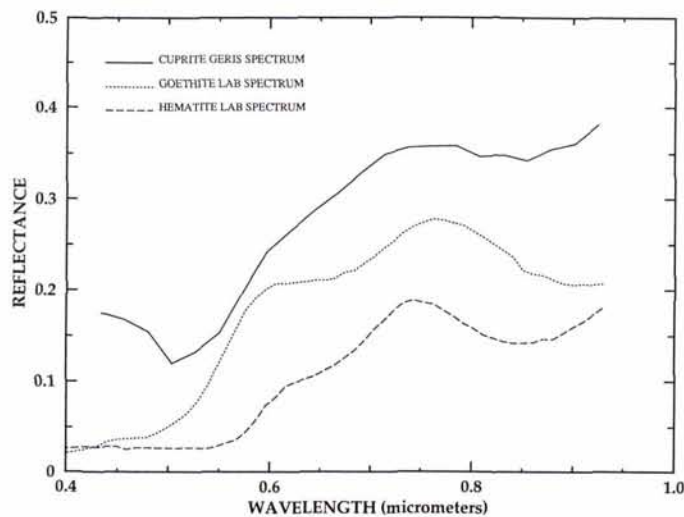
FIG. 12. Comparison of laboratory spectra of hematite and goethite and a GERIS spectrum from Cuprite, Nevada, interpreted to contain hematite. This result has not yet been verified by collection of field samples. Note the match of the broad absorption feature near 0.85 µm in the GERIS and hematite spectrum. The cause for the mismatch in slope between the GERIS and the other spectra between 0.4 and 0.5 µm is not known, but may be caused by low signal-to-noise in this region. The spectra are offset vertically for clarity and the absolute values of the reflectance axis do not show true brightness.

served. A central silica cap mapped previously by Abrams *et al.* (1977) (Figure 4) was not distinguished using spectral classification of the 63-channel imaging spectrometer data because spectra of the cap were highly variable and no characteristic spectrum could be identified. The silica cap can be seen, however, as a bright, unclassified area in the center of Plate 2. The imaging spectrometer data show that the first zone out from the silica cap consists primarily of alunite (Blue on Plate 2). This corresponds with portions of the opalized zone mapped by Abrams *et al.* (1977). A kaolinitic zone is found generally farther from the center (Red on Plate 2), but overlapping the alunite zone. This zone corresponds in part with the argillized zone of Abrams; however, it is much more extensive than shown on Figure 4. Because Abrams defined his argillized zone on the basis of kaolinite, and kaolinite is difficult to map in the field, it is likely that the distribution shown in Plate 2 is representative of the extent of the argillized zone. It should also be noted, however, that many of the areas mapped as kaolinitic using the imaging spectrometer data that have high spatial variability correspond to obvious alluvial fan surfaces, indicating transported kaolinite derived from altered areas. Significant occurrences of alunite and kaolinite are also mapped west of U. S. Highway 95; however, these exposures are outside the area of mapped alteration and have not yet been evaluated in the field. Areas of ammonium enrichment near the northwest edge of the former hydrothermal system were also identified by using the GERIS data to detect the presence of the mineral buddingtonite (Green on Plate 2). Buddingtonite is an ammonium-bearing feldspar discovered in the Cuprite district using the NASA Airborne Imaging Spectrometer (AIS) (Goetz and Srivastava, 1985). Buddingtonite is very difficult to recognize in the field but was found using the imaging spectrometer data by the presence of a broad 2.117 µm absorption band and a secondary narrow band near 2.02 µm (Krohn and Altaner, 1987). Hematite mapped using the GERIS data (Purple in Plate 3) is distributed primarily around the contact between the altered and unaltered volcanic rocks.

DISCUSSION

Imaging spectrometer data provide a fast yet accurate means of mapping mineralogy at the Earth's surface. Zoned mineralogy mapped at Cuprite, Nevada, using the GERIS system, conforms in a general sense to previous field and multispectral image mapping; however, identification of individual minerals and spatial display of the dominant mineralogy adds information that can be used to help determine the morphology and genetic origin of the hydrothermal system. The zoning at Cuprite has many characteristics similar to those described for large replacement-type alunite deposits. Hall and Bauer (1983) describe four principal alteration zones consisting both radially and with increasing depth of (1) an interior silceous core or cap zone, (2) a Quartz-alunite zone (*alunite* and microcrystalline quartz), (3) an Argillic Zone (*kaolinite* and dickite), and (4) a Propylitic Zone (epidote, chlorite, *zeolites*, pyrite, and calcite). This zoning is idealized and actual systems exhibit irregular and inhomogeneous zoning assemblages; however, the Cuprite zoning mapped using the GERIS system is remarkably like that described above. Identification and mapping of the ammonium feldspar buddingtonite using the GERIS system is also significant because this mineral is often associated with hot springs type gold deposits (Krohn, 1986).

The minerals present in this typical alunite zoned-replacement deposit indicate a sulfuric acid-charged system with hydrothermal fluids and solfataric gases emitted in a "hot springs" type volcanic environment (Hall and Bauer, 1983). Deep recirculation of meteoric water in a convection cell above an intrusive body resulted in replacement of primary rock forming minerals with the alteration minerals observed at Cuprite. The classical bullseye zoning at Cuprite indicates that alteration probably occurred along a localized vent with the lateral distribution controlled by the rock textures and porosity. Mineral zoning was controlled by decreasing acidity and temperature with increasing distance from the conduit structure.

Hall and Bauer (1983) cite numerous examples of the correlation between alunite and hypogene metalliferous deposits. The presence of alunite at the surface presents a favorable target for further gold exploration at depth and in peripheral alteration zones. This research demonstrates that imaging spectrometers can be a viable part of a precious metals exploration effort. Integrated use of satellite remote sensing and selected imaging spectrometer aircraft coverage can be a powerful tool in guiding the initial stages of property assessment and development.

ACKNOWLEDGMENTS

REFERENCES

Abrams, M. J., R. P. Ashley, L. C. Rowan, A. F. H. Goetz and A. B. Kahle, 1977. Mapping of hydrothermal alteration in the Cuprite mining district, Nevada using aircraft scanner images for the spectral region 0.46-2.36 µm, *Geology*, Vol. 5, pp. 713–718.

Ashley, R. P., and M. J. Abrams, 1980. *Alteration Mapping Using Multispectral Images-Cuprite Mining District, Esmeralda County, Nevada*: U. S. Geological Survey Open File Report 80–367, 17p.

Boardman, J. W., 1989. Spectral and spatial unmixing: Applications of singular value decomposition: *Proceedings, Image Processing '89*, 23–26 May 1989, Sparks, Nevada (in press).

Clark, R. N., King, T. V. V., and Gorelick, N. S., 1987. Automatic continuum analysis of reflectance spectra: *Proceedings, Third AIS*

workshop, 2-4 June 1987, JPL Publication 87-30, Jet Propulsion Laboratory, Pasadena, California, pp. 138–142.

Curtiss, Brian, M. O. Smith, and J. B. Adams, 1985. Separation of hydrothermal Fe (III) oxyhydroxides from weathering produced Fe (III) oxyhydroxides in multispectral images (Abst.): *Proceedings, International Symposium on Remote Sensing of Environment, Fourth Thematic Conference, "Remote Sensing for Exploration Geology"*, San Francisco, California, 1-4 April, 1985, Environmental Research Institute of Michigan, Ann Arbor, 497 p.

Ehmann, W. J., and Norma Vergo, 1986. Spectral discrimination of zeolites and dioctahedral clays in the near-infrared: *Proceedings, International Symposium on Remote Sensing of Environment, Fifth Thematic Conference, "Remote Sensing for Exploration Geology"*, Reno, Nevada, 29 September − 2 October 1986, Environmental Research Institute of Michigan, Ann Arbor, pp. 417–425.

Elvidge, C. D., 1988. Vegetation reflectance features in AVIRIS data: *Proceedings, International Symposium on Remote Sensing of Environment, Sixth Thematic Conference, "Remote Sensing for Exploration Geology"*, Houston, Tx, 16 − 19 May, 1988, Environmental Research Institute of Michigan, Ann Arbor, p. 169–182.

Gillespie, A. R., A. B. Kahle, and R. E. Walker, 1986. Color enhancement of highly correlated images. I. Decorrelation and HSI contrast stretches: *Remote Sensing of Environment*, Vol. 20, pp. 209–235.

Goetz, A. F. H., and Vinay Strivastava, 1985. Mineralogical mapping in the Cuprite mining district: *Proceedings of the Airborne Imaging Spectrometer (AIS) Data Analysis Workshop*, 8-10 April 1985, JPL Publication 85-41, Jet Propulsion Laboratory, Pasadena, California, pp. 22–29.

Goetz, A. F. H., Gregg Vane, J. E. Solomon, and B. N. Rock, 1985. Imaging spectrometry for earth remote sensing: *Science*, Vol. 228, pp. 1147–1153.

Green, A. A., and M. D. Craig, 1985. Analysis of aircraft spectrometer data with logarithmic residuals: *Proceedings, AIS workshop*, 8-10 April 1985, JPL Publication 85-41, Jet Propulsion Laboratory, Pasadena, California, pp. 111–119.

Hall, R. B., and C. W. Bauer, 1983. Alunite: *Industrial Minerals and Rocks*, 5th edition (S. J. Lefond, ed.), AIME, pp. 417–434.

Kahle, A. B., and A. F. H. Goetz, 1983. Mineralogical information from a new airborne thermal infrared multispectral scanner: *Science*, Vol. 222, No. 4619, pp. 24–27.

Kneisyz, F. X., E. P. Shettle, W. P. Gallery, J. H. Chetwynd, Jr., L. W. Abreu, J. E. A. Selby, R. W. Fen, and R. A. McClatchey, 1980. *Atmospheric transmittance/radiance: Computer Code LOWTRAN*: AFCRL Environmental Research Paper No. 697, AFCRL-80-0067.

Krohn, M. D., 1986. Spectral properties (.4 to 25 microns) of selected rocks associated with disseminated gold and silver deposits in Nevada and Idaho: *Journal of Geophysical Research*, Vol. 91B, No. 1, pp. 767–783.

Krohn, M. D., and S. P. Altaner, 1987. Near-infrared detection of ammonium minerals: *Geophysics*, Vol. 52, No. 7, pp. 924–930.

Kruse, F. A., 1987. Extracting spectral information from imaging spectrometer data: A case history from the northern Grapevine Mountains, Nevada/California: *Proceedings, 31st Annual International Technical Symposium*, 16-21 August 1987, SPIE Proceedings, Imaging Spectroscopy II, Vol. 834, pp. 119–128.

———, 1988. Use of Airborne Imaging Spectrometer data to map minerals associated with hydrothermally altered rocks in the northern Grapevine Mountains, Nevada and California: *Remote Sensing of Environment*, Vol. 24, No. 1, pp. 31–51.

Kruse, F. A., W. M. Calvin, and Olivier Seznec, 1988. Automated extraction of absorption features from Airborne Visible/Infrared Imaging Spectrometer (AVIRIS) and Geophysical Environmental Research imaging spectrometer (GERIS) data: *Proceedings AVIRIS Performance Evaluation Workshop*, JPL publication 83-38, Jet Propulsion Laboratory, Pasadena, California, pp. 62–75.

Kruse, F. A., D. H. Knepper, Jr., and R. N. Clark, 1986. Use of digital Munsell color space to assist interpretation of imaging spectrometer data — Geologic examples from the northern Grapevine Mountains, California and Nevada: *Proceedings, 2nd AIS Data Analysis Workshop, Pasadena*, California 6-8 May 1986, JPL Publication 86-35, Jet Propulsion Laboratoy, Pasadena, California, pp. 132–137.

Kruse, F. A., and G. L. Raines, 1984. A technique for enhancing digital color images by contrast stretching in Munsell color space: *Proceedings, International Symposium on Remote Sensing of Environment, Third Thematic Conference, "Remote Sensing for Exploration Geology"*, Colorado Springs, Colorado, 16-19 April 1984, pp. 755–760.

Kruse, F. A., G. L. Raines, and Kenneth Watson, 1985. Analytical techniques for extracting geologic information from multichannel airborne spectroradiometer and airborne imaging spectrometer data: *Proceedings, International Symposium on Remote Sensing of Environment, Fourth Thematic Conference, "Remote Sensing for Exploration Geology"*, San Francisco, California, 1-4 April 1985, pp. 309–324.

Lang, H. R., S. L. Adams, J. E. Conel, B. A. McGuffie, E. D. Paylor, and R. E. Walker, 1987. Multispectral remote sensing as stratigraphic tool, Wind River Basin and Big Horn Basin areas, Wyoming: *AAPG Bulletin*, Vol. 71, No. 4, pp. 389–402.

Marsh, S. E., and J. B. McKeon, 1983. Integrated analysis of high-resolution field and airborne spectroradiometer data for alteration mapping: *Economic Geology*, Vol. 78, No. 4, pp. 618–632.

Mazer, A.S., Miki Martin, Meemong Lee, and J. E. Solomon, 1987. Image processing software for imaging spectrometry: *Proceedings, 31st Annual International Technical Symposium*, 16-21 August, 1987, Society of Photo-Optical Instrumentation Engineers, Vol. 834, pp. 136–139.

———, 1988. Image processing software for imaging spectrometry data analysis: *Remote Sensing of Environment*, Vol. 24, No. 1, pp. 201–210.

Mustard, J. F., and C. M. Pieters, 1986. Abundance and distribution of mineral components associated with Moses Rock (Kimberlite) diatreme: *Proceedings, 2nd Airborne Imaging Spectrometer (AIS) Data Analysis Workshop*, 6-8 May 1986, JPL Publication 86-35, Jet Propulsion Laboratory, Pasadena, California, pp. 81–85.

———, 1987. Abundance and distribution of ultramafic microbreccia in Moses Rock Dike: Quantitative application of mapping spectroscopy: *Journal of Geophysical Research*, Vol. 92, No. B10, pp. 10376–10390.

Pieters, C. M., and J. F. Mustard, 1988. Exploration of crustal/mantle material for the Earth and Moon using reflectance spectroscopy: *Remote Sensing of Environment*, Vol. 24, No. 1, pp. 151–178.

Porter, W. M., and H. T. Enmark, 1987. A system overview of the Airborne Visible/Infrared Imaging Spectrometer (AVIRIS): *Proceedings, 31st Annual International Technical Symposium*, 16-21 August 1987, Society of Photo-Optical Instrumentation Engineers, Vol. 834, pp. 22–31.

Roberts, D. A., Y. Yamaguchi, and R. J. P. Lyon, 1985. Calibration of Airborne Imaging Spectrometer Data to percent reflectance using field spectral measurements: *Proceedings, Nineteenth International Symposium on Remote Sensing of Environment*, Ann Arbor, Michigan, 21-25 October 1985.

Rowan, L. C., P. H. Wetlaufer, A. F. H. Goetz, F. C. Billingsley, and J. H. Stewart, 1974. *Discrimination of Rock Types and Detection of Hydrothermally Altered Areas in South-Central Nevada by the use of Computer Enhanced ERTS Images*, U. S. Geological Survey Professional Paper 883, 35 p.

Shipman, Hugh, and J. B. Adams, 1987. Detectability of minerals on desert alluvial fans using reflectance spectra: *Journal of Geophysical Research*, vol. 92, No, B10, pp. 10391–10402.

Smith, M. O., and J. B. Adams, 1985. Interpretation of AIS images of Cuprite, Nevada using constraints of spectral mixtures: *Proceedings, AIS workshop*, 8-10 April 1985, JPL Publication 85-41, Jet Propulsion Laboratory, Pasadena, California, pp. 62–67.

Torson, J. M., 1989. Interactive image cube visualization and analysis: *Proceedings, Chapel Hill Workshop on Volume Visualization*, 18-19 May 1989, University of North Carolina at Chapel Hill, (in press).

Vane, Gregg (ed.), 1987a. *Proceedings of the 3rd Airborne Imaging Spectrometer (AIS) Data Analysis Workshop*, 2-4 June 1987, JPL Publication 87-30, Jet Propulsion Laboratory, Pasadena, California, 183 p.

———, 1987b. First results from the Airborne Visible/Infrared Imaging Spectrometer (AVIRIS): *Proceedings, 31st Annual International Technical Symposium*, 16-21 August, 1987, Society of Photo-Optical Instrumentation Engineers, Vol. 834, pp. 166–174.

Vane, Gregg, and A. F. H. Goetz (eds.), 1985. *Proceedings of the Airborne*

Imaging Spectrometer (AIS) Data Analysis Workshop, 8-10 April 1985, JPL Publication 85-41, Jet Propulsion Laboratory, Pasadena, California, 173 p.

————, 1986. *Proceedings of the 2nd Airborne Imaging Spectrometer (AIS) Data Analysis Workshop*, 6-8 May 1986, JPL Publication 86-35, Jet Propulsion Laboratory, Pasadena, California, 212 p.

Vane, Gregg, A. F. H. Goetz, and J. B. Wellman, 1983. Airborne imaging spectrometer: A New Tool for Remote Sensing: *IEEE Trans-*

actions on Geoscience and Remote Sensing, Vol. GE-22, No. 6, pp. 546–549.

Yamaguchi, Yasushi, and R. J. P. Lyon, 1986. Identification of clay minerals by feature coding of near-infrared spectra: *Proceedings, International Symposium on Remote Sensing of Environment, Fifth Thematic Conference, "Remote Sensing for Exploration Geology"*, Reno, Nevada, 29 September- 2 October 1986, Environmental Research Institute of Michigan, Ann Arbor, pp. 627–636.

Forum

Comparison of Landsat MSS Pixel Array Sizes for Estimating Water Quality

I RECENTLY ran across a paper that appeared in this journal (Ritchie and Cooper, *PE&RS*, November 1987, pp. 1549–1553) on which I would like to comment.

In that paper, 5 by 5 square pixel arrays from Landsat MSS data for the area including Moon Lake in Mississippi were compared with total suspended solids and chlorophyll-a readings taken from the same locations. From each array, subarrays were formed by using the center pixel, all four 2 by 2 center pixels, the middle 3 by 3, and the 5 by 5 pixels (see Figure 1). These were compared with the purpose of being able to state what size subarray was best, or at least which were inadequate. I would like to point out some shortcomings with their analysis.

One of the problems with Ritchie and Cooper's method of analysis is that it treats very non-independent observations as though they were independent; that is, the data from the subarrays overlap either completely or to a great extent. We would expect more difference between non-overlapping subarrays. For

example, in order for a 2 by 2 and the 3 by 3 subarrays to be different the 2 by 2 would have to be different from the non-overlapping part of the 3 by 3. Similarly, comparing the 3 by 3 with the 5 by 5 is equivalent to comparing the 3 by 3 with the 16 pixels on the outer ring of the array. In fact, what the Ritchie and Cooper analysis does essentially is to compare the mean responses from the center, middle ring, and outer rings of the array. In other words, whether the measurements taken in the middle of the array are different from those towards the sides. An analysis of these data sets would be valid and would answer the same question in a more precise manner. It also suggests that the rows and the lines could be compared or whatever other subarrays make sense for technical reasons.

Another problem is the interpretation of the results. Ritchie and Cooper do all possible pair-wise t-tests to infer whether the means of the different subarrays are different. There seems to be a confusion here regarding the difference between parameters and estimates. Over an area there is a mean chlorophyll-a level. If we then take four pixel readings or nine from this area we are taking samples from a single population. The sample means from these four and nine readings are estimating the same population mean. Any statistical difference must arise strictly by chance. That is, if we do a number of separate t-tests and claim the two sample means are different at the 10 percent significance level, then if the t-tests are independent we would expect about 10 percent of them to be significant even if there is no real difference between the population means the sample means are estimating. However, not only are the t-tests Ritchie and Cooper performing not independent but as seen above the means are not independent either. So that it should not be surprising if many (or few) of the tests are significant. For example, they find that one of the 2 by 2 subarray means is significantly different from both the 3 by 3 and the 5 by 5, but because most of the data in the 5 by 5 is in the 3 by 3, then the fact that the 2 by 2 is different from the 3 by 3 increases the chances that it will also be different from the 5 by 5 array.

The question that should be addressed, then, is not whether different subarray sizes give different expected readings (they will not under the assumption of a well calibrated instrument), but how much better the larger subarrays are than the smaller ones. This will depend on the within-site variance between the pixels. There is no answer to which size is "significantly" more accurate than another.
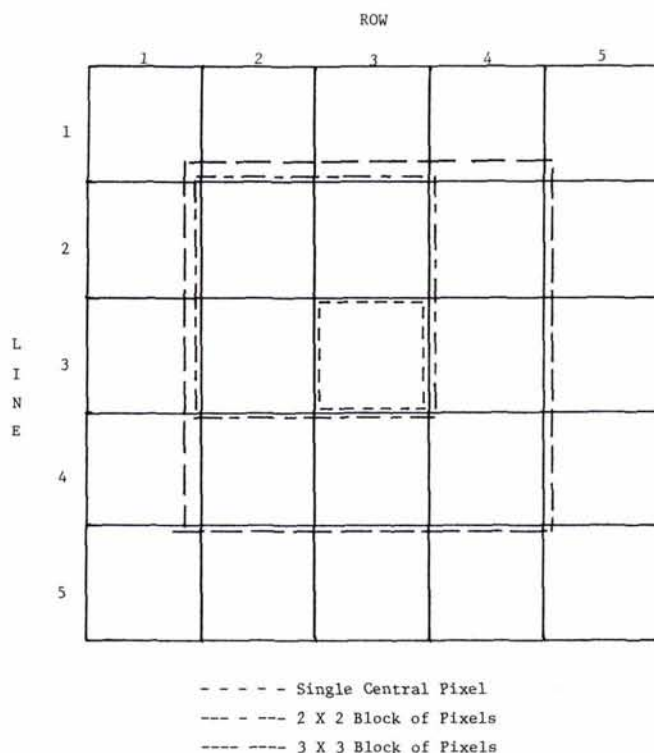

FIG. 1. Schematic diagram showing the relation between the different pixel arrays. From Ritchie and Cooper.

—*Michael H. Ames*
Department of Experimental Statistics
Box 30003, Dept. 3130
New Mexico State University
Las Cruces, NM 88003-0003